Motion Correction of ^{18}F-NaF PET for Imaging Coronary Atherosclerotic Plaques

Mathieu Rubeaux[1], Nikhil V. Joshi[2], Marc R. Dweck[2], Alison Fletcher[2], Manish Motwani[1], Louise E. Thomson[1], Guido Germano[1], Damini Dey[1], Debiao Li[1], Daniel S. Berman[1], David E. Newby[2], and Piotr J. Slomka[1]

[1]*Cedars-Sinai Medical Center, Los Angeles, California; and* [2]*University of Edinburgh, Edinburgh, United Kingdom*

Ruptured coronary atherosclerotic plaques commonly cause acute myocardial infarction. It has recently been shown that active microcalcification in the coronary arteries, one of the features that characterizes vulnerable plaques at risk of rupture, can be imaged using ^{18}F-NaF PET. We aimed to determine whether a motion correction technique applied to gated ^{18}F-NaF PET images could enhance image quality and improve uptake estimates. **Methods:** Seventeen patients with myocardial infarction ($n = 7$) or stable angina ($n = 10$) underwent ^{18}F-NaF PET and prospective coronary CT angiography. PET data were reconstructed in 4 different ways: the first was 1 gated bin (end-diastolic phase with 25% of the counts), the second was 4 gated bins (consecutive 25% segments), the third was 10 gated bins (consecutive 10% segments), and the fourth was ungated. Subsequently, with data from either 4 or 10 bins, gated PET images were registered using a local, nonlinear motion correction method guided by the extracted coronary arteries from CT angiography. Global noise levels and target-to-background ratios (TBR) defined on manually delineated coronary plaque lesions were compared to assess image quality and uptake estimates. **Results:** Compared with the reference standard of using only 1 bin of PET data, motion correction using 10 bins of PET data reduced image noise by 46% ($P < 0.0001$). TBR in positive lesions for 10-bin motion-corrected data was 11% higher than for 1-bin data (1.98 [interquartile range, 1.70–2.37] vs. 1.78 [1.58–2.16], $P = 0.0027$) and 33% higher than for ungated data (1.98 [1.70–2.37] vs. 1.49 [1.39–1.88], $P < 0.0001$). **Conclusion:** Motion correction of gated ^{18}F-NaF PET/coronary CT angiography is feasible, reduces image noise, and increases TBR. This improvement may allow more reliable identification of vulnerable coronary artery plaques using ^{18}F-NaF PET.

Key Words: motion correction; ^{18}F-sodium fluoride PET; ^{18}F-NaF; coronary atherosclerotic plaques; microcalcification

J Nucl Med 2016; 57:54–59
DOI: 10.2967/jnumed.115.162990

Acute myocardial infarction (MI) is the leading cause of death in the United States, with 735,000 Americans experiencing an acute MI and about 120,000 dying as a consequence each year (*1*). Acute MI most commonly results from coronary atherosclerotic plaque rupture. Despite this cause, current treatment algorithms make no allowance for the presence or absence of vulnerable plaques at risk of rupture, and the current dogma is to treat all patients with any atherosclerosis in the same way. An accurate, noninvasive, a priori method for identifying such rupture-prone plaques would challenge this dogma, allowing high-risk patients to be selectively targeted with patient-specific therapies.

Histopathologic studies of patients who died from acute MI have demonstrated that the plaques that have ruptured and caused acute MI have several common characteristics. Among these, microcalcification is a consistent finding, believed to represent the very early stages of the body's attempt to heal inflamed necrotic plaque. A recent series of studies (*2–4*) demonstrated that ^{18}F-sodium fluoride (^{18}F-NaF)—an inexpensive, Food and Drug Administration–approved, widely available PET tracer—binds preferentially to regions of vascular microcalcification and can be used to identify high-risk plaques and plaque rupture in the coronary arteries. In particular, in a study by Joshi et al. increased ^{18}F-NaF PET activity was found to localize to the exact site of plaque rupture in more than 90% of patients who had recently experienced an acute MI, independent of stenting (*2*).

There are, however, several important limitations still to be addressed. The difference in target-to-background ratio (TBR) between culprit plaques (implicated in acute MI) and nonculprit plaques in ^{18}F-NaF PET is relatively small (~34%) because of blurring of coronary uptake by cardiac, respiratory, and patient motion. The implication is a greater risk of misclassification when this technique is applied to real-world, unselected populations. Unfortunately, recent general-purpose motion correction methods proposed for PET (*5,6*) are not applicable because of lack of clear anatomic landmarks in the heart region on the ^{18}F-NaF scan. To partially address the problem of motion, only a single cardiac phase (representing about 25% of the PET data) was used in the initial study (*2*), at the expense of a significant increase in noise. Although this was a useful exploratory strategy, the combination of an already-narrow diagnostic TBR margin and increased noise is clearly suboptimal.

We previously developed motion correction techniques for cardiac perfusion data from SPECT and PET, which facilitated an increase in image contrast compared with ungated data (*7,8*). In the present study, we aimed to overcome some of the current limitations of ^{18}F-NaF PET by developing a motion correction method for coronary ^{18}F-NaF PET to optimize this promising plaque-imaging technique.

MATERIALS AND METHODS

Patients

Patients were recruited from the Royal Infirmary of Edinburgh between February 2012 and January 2013 in 2 cohorts: 7 patients with acute ST-segment or non–ST-segment elevation acute MI and 10

Received Jun. 30, 2015; revision accepted Oct. 5, 2015.
For correspondence or reprints contact: Piotr J. Slomka, Artificial Intelligence in Medicine Program, 8700 Beverly Blvd., Ste. A047N, Los Angeles, CA 90048.
E-mail: piotr.slomka@cshs.org
Published online Oct. 15, 2015.

patients with stable angina pectoris undergoing elective invasive coronary angiography. Table 1 shows the demographic and clinical characteristics of these patients. All underwent a comprehensive baseline clinical assessment, including evaluation of their cardiovascular risk factor profile. Studies were done with the approval of the local research ethics committee, in accordance with the Declaration of Helsinki, and with the written informed consent of each participant.

Imaging and Analysis Protocols

All patients underwent ^{18}F-NaF PET/CT imaging of the coronary arteries with cardiac gating on a hybrid scanner (64-detector Biograph mCT; Siemens Medical Systems). The subjects were administered a target dose of 125 MBq of ^{18}F-NaF intravenously and subsequently rested in a quiet environment for 60 min. An attenuation correction CT scan (nonenhanced, 120 kV and 50 mA) was then obtained, followed by PET imaging of the thorax in list-mode for 20 min.

Prospectively gated coronary CT angiography (CCTA) was undertaken during the same visit as the ^{18}F-NaF scan, using a 330-ms rotation time, a 100-kV (body mass index $<$ 25 kg/m^2) or 120-kV (body mass index $>$ 25 kg/m^2) tube voltage, a 160- to 245-mAs tube current, and a 3.8-mm/rotation table feed, with prospective electrocardiography triggering (heart rate regular and $<$ 60 beats/min), or retrospective electrocardiography gating (heart rate $>$ 60 beats/min). Depending on the body mass index, a bolus of 80–100 mL of contrast material (400 mg I/mL, Iomeron; Bracco) was injected intravenously at 5 mL/s, after determining the appropriate trigger delay with a test bolus of 20 mL of contrast material. Electrocardiography-gated PET images were reconstructed using the Siemens Ultra-HD algorithm (time-of-flight plus point spread function) in multiple phases of the cardiac cycle. For this study, 4 different sets of data were reconstructed from list-mode data: 1 bin with 25% of the counts during the end-diastolic phase (the technique used in the original study of Joshi et al. (*2*)), 4 bins, 10 bins, and ungated. The PET pixel size was 2 mm. The CCTA scans were reconstructed at 0.75 × 0.7 mm and 0.6 × 0.3 mm for retrospective and prospective acquisitions, respectively, at 70% of the cardiac cycle.

Motion Correction

The goal of the motion correction procedure was to compensate for coronary artery motion in the different phases of the electrocardiography-gated PET data. Gated PET with 4 and 10 time bins were reconstructed from the PET list-mode files. The registration aimed to align all bins to the end-diastolic phase position, synchronizing the registered data to the prospective CCTA and, for comparison purposes, to the 1-bin PET data corresponding to the end-diastolic phase (as used in the original study). The end-diastolic phase, taken as the reference, corresponded to bin 3 in the dataset with 4 bins and to bin 7 in the dataset with 10 bins.

TABLE 1
Patients' Demographic and Clinical Characteristics

Parameter	Stable angina (n = 10)	MI (n = 7)
Mean age ± SD (y)	67 ± 9	66 ± 7
Men (n)	9 (90%)	7 (100%)
Mean BMI ± SD (kg/m^2)	29 ± 5	28 ± 8
Agatston score		
Median	1,010	498
IQR	560–2,175	355–771
History (n)		
MI	4 (40%)	0
PCI	5 (50%)	1 (14%)
CABG	5 (50%)	0
Lesions (n)	31 (61%)	20 (39%)
Positive	19 (68%)	9 (32%)
Negative	12 (52%)	11 (48%)

BMI = body mass index; MI = myocardial infarction; PCI = percutaneous coronary intervention; CABG = coronary artery bypass graft.

The registration of individual bins of ^{18}F-NaF PET presents a unique challenge because there are no clear anatomic references near the heart, and motion of bones (where there is significant ^{18}F-NaF uptake) does not correlate with motion of the heart. Thus, innovative approaches are required to deal with this problem. The procedure we used is illustrated in Figure 1. To recover the anatomic information that is missing in the PET data, we used the CCTA data that clearly delineate the coronary arteries. The end-expiration position of the CCTA allowed excellent alignment with PET data when the patient remained in the same position. Coronary regions were first extracted from the CCTA by vessel tracking based on Bayesian maximal paths (*9*), as implemented and validated in our Autoplaq CCTA processing software (*10–12*). This algorithm requires as input only proximal and distal points for every coronary artery and automatically finds the vessel centerline. The centerlines of the right, left circumflex, and left anterior descending coronary arteries were extracted for every patient in this manner.

Subsequently, the centerline coordinates were transferred to the PET volumes to automatically extract 3-dimensional tubular volumes of interest surrounding the coronary arteries in the gated PET images, defined by a 20-mm radius around each centerline. This radius was chosen to take into account the maximum displacement that can occur during the cardiac cycle, also allowing for potential remaining misregistration. Techniques that did not constrain the registration by coronary vessel regions were hampered by noise adjacent to the coronary arteries.

Next, a nonlinear level-set algorithm (*13*) was applied to the extracted coronary regions and constrained according to the expected coronary artery motion. Every volume of interest of the PET data from each bin was then registered to the end-diastolic reference artery region. The advantage of this method over other nonlinear registration techniques is the computational efficiency and knowledge-based estimation of the expected arterial motion. After the registration process, all registered volumes of interest were inserted back into their original PET image, using a linear gradient at the border between the registered volume of interest and the nonregistered original PET image to blend both volumes and ensure smooth transition between the regions. Finally, all registered PET images were summed into a single volume. In this manner, we obtained static 4- and 10-bin motion-corrected PET data.

Lesion and TBR

To define the lesions, the PET data were fused with the CCTA data and analyzed on an OsiriX workstation (OsiriX Imaging Software) by experienced observers masked to the clinical diagnosis. Two-dimensional regions of interest were drawn around all major (diameter $>$ 2 mm) epicardial vessels on 3-mm axial slices just beyond the discernible adventitial border. We used a previously established 95% lower reference limit to categorize coronary plaques into ^{18}F-NaF–positive and –negative lesions, on the end-diastolic data as in the original study. Focal uptake with a target-to-background ratio (TBR) more than 25% higher than a proximal reference lesion were categorized as ^{18}F-NaF–positive plaques, whereas plaques were considered ^{18}F-NaF–negative if these criteria were not achieved. This limit was based on our previous study, in which plaques with high ^{18}F-NaF uptake had maximum TBRs that were 44% (95% confidence interval, 26–62) higher than a proximal quiescent reference lesion (*3*).

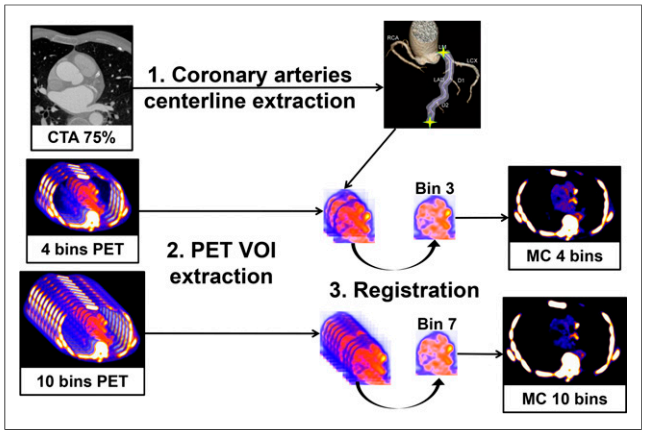

FIGURE 1. Overview of the motion correction method. (1) Coronary artery centerlines are extracted from CCTA in end-diastolic phase using CCTA analysis software. (2) Volumes of interest surrounding coronary arteries are extracted from 4- and 10-bin PET data using previously extracted CCTA centerlines. (3) All bins of data are registered to the common end-diastolic reference bin (bins 3 and 7 for 4- and 10-bin data, respectively) by nonlinear level-set registration restricted to coronary regions. Then, registered VOIs are inserted back into their original PET volumes, and all registered PET images are summed into a single volume to obtain motion-corrected 4- and 10-bin data. MC = motion-corrected; VOI = volume of interest.

TBR was defined as the ratio of the maximum activity values in the manually defined lesion to the mean value of the background, taken to be the blood pool in the middle of the left ventricle. This region was positioned to include the whole blood pool region in a midventricular slice for each patient. The noise was determined as the ratio of the mean to the SD of the background.

Statistical Analysis

Statistical analyses were performed with Analyze-it software. For all continuous variables, the Shapiro–Wilk test was used to assess normality. All continuous variables were described as mean ± SD or median and interquartile range (IQR). Nonparametric results were presented as median and IQR and compared using the Wilcoxon signed-rank test as appropriate. A 2-sided P value of less than 0.05 was taken as statistically significant.

RESULTS

Patients were predominantly middle-aged men and had multiple cardiovascular risk factors (Table 1). Radiation exposure for CCTA and PET is summarized in Table 2. The algorithm successfully registered the gated data for all studies, as assessed visually in the cinematic display. The approximate processing time was about 1 min/study. The results were computed and compared for the 4 sets of reconstructed data: 1 single PET bin corresponding to the end-diastolic phase, as presented in the initial trial (*2*); 4 and 10 bins that were motion-corrected as described above; and ungated data. In total, 51 lesions (28 positive, 23 negative) were delineated in the 17 patients. These lesions were distributed over the major coronary arteries: 17 (33%) in the left anterior descending coronary artery, 21 (41%) in the right coronary artery, and 13 (26%) in the left circumflex coronary artery. The TBR in positive and negative lesions was measured in the 4 sets of data.

Activity

^{18}F-NaF activity (expressed as TBR) in the positive lesions with 10-bin motion-corrected data was 11% higher than with 1-bin data (1.98 [IQR, 1.70–2.37] vs. 1.78 [IQR, 1.58–2.16], $P = 0.0027$) and 33% higher than with ungated data (1.98 [IQR, 1.70–2.37] vs. 1.49 [IQR, 1.39–1.88], $P < 0.0001$). In contrast, no difference was observed when comparing 1- to 4-bin motion-corrected data (1.78 [IQR, 1.58–2.16] vs. 1.75 [IQR, 1.50–2.16], $P = 0.77$) (Fig. 2A).

In ^{18}F-NaF–negative lesions, we observed some differences between 1- and 4-bin motion-corrected data (0.90 [IQR, 0.70–1.05] vs. 0.91 [IQR, 0.76–1.09], $P = 0.006$) as well as between 1- and 10-bin motion-corrected data (0.90 [IQR, 0.70–1.05] vs. 0.93 [IQR, 0.80–1.04], $P = 0.025$) (Fig. 2B), but these absolute differences were much smaller than for the ^{18}F-NaF–positive lesions. Furthermore, the median TBRs in the ^{18}F-NaF–negative lesions were less than 1.0 for all techniques.

Overall, the median TBR difference between ^{18}F-NaF–positive and –negative lesions increased from 0.88 to 1.05 using the 10-bin motion-corrected data, as compared with 1 bin. This technique should therefore allow for better discrimination between positive and negative lesions, as compared with the single end-diastolic bin alone that was presented in the original trial (*2*).

Noise

Noise was significantly reduced by using the 4- or 10-bin motion correction method as compared with the single end-diastolic bin: 0.09 [IQR, 0.08–0.12] vs. 0.18 [IQR, 0.15–0.24], $P < 0.0001$ (Fig. 2C). This is an expected finding since only 25% of the PET counts were used in the 1-bin data. Noise was essentially the same for ungated data and motion-corrected 4- and 10-bin data since all the PET counts were used by these 3 techniques.

Example images illustrating the noise decrease and TBR improvement are shown in Figure 3.

TABLE 2
Patients' Radiation Exposure (mSv) During Study

Parameter	^{18}F-NaF	CCTA dose	AC CT dose	PET/CT + CCTA
Prospective				
Range	2.8–3.1	1.3–5.8	0.5–1.8	4.7–9.9
Mean ± SD	2.9 ± 0.1	3.4 ± 1.2	1.0 ± 0.4	7.3 ± 1.4
Retrospective				
Range	2.8–3.0	7.8–12.7	0.9–1.1	11.6–16.7
Mean ± SD	2.9 ± 0.1	9.7 ± 2.7	1.0 ± 0.1	13.6 ± 2.7

Conversion factors are 0.014 mSv/mGy·cm for CCTA and attenuation-corrected (AC) CT and 0.024 mSv/MBq for ^{18}F-NaF.

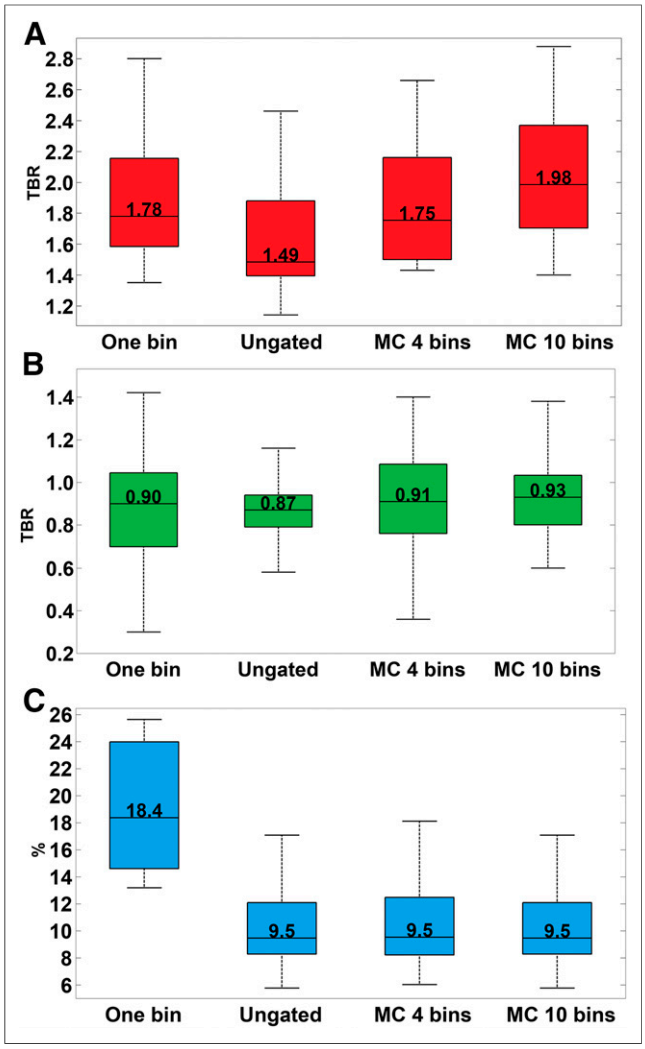

FIGURE 2. TBRs in positive (A) and negative (B) lesions and noise (C) are shown for different PET datasets (1-bin data, ungated data, motion-corrected data created from 4 bins, and motion-corrected data created from 10 bins). (A) TBR in positive lesions increases with motion correction for 10-bin data, as compared with 1-bin data and ungated data. (B) TBR in negative lesions remains below 1 using motion correction. (C) Noise is almost halved using motion correction, as compared with 1-bin data. MC = motion-corrected.

Motion

We also computed the maximal motion of plaques in the different coronary arteries that occurred during the motion correction process. The median end-systolic–to–end-diastolic displacement was 17.2 mm [IQR, 14.6–19.0 mm] in the left anterior descending coronary artery, 17.7 mm [IQR, 16.1–20.7 mm] in the left circumflex coronary artery, and 19.4 mm [IQR, 16.2–22 mm] in the right coronary artery. These results agree with the range of the coronary motion during the cardiac cycle that has been reported in the literature (*14*).

DISCUSSION

We have developed a method to correct coronary motion in ^{18}F-NaF PET imaging data by applying level-set–based nonlinear PET registration of individual PET time-bins to the end-diastolic position. This registration was constrained to the coronary regions extracted from the coregistered CCTA data to avoid registration to spurious noise signals outside the coronary regions. As compared with the original method (*2*), the new method demonstrated increased TBRs while drastically reducing noise (Fig. 3B). The best results were obtained for the 10-bin motion-corrected data since those data provided the best time-resolved motion correction.

Previous studies have addressed cardiac motion correction in PET and SPECT (*7,8*). Dual gating (cardiac/respiratory) (*15,16*) and dual correction have been reported by several groups (*5,6,17,18*). However, all of these methods depend on uptake in anatomic organs (in the case of cardiac imaging, the myocardium) and therefore are not applicable to coronary PET. ^{18}F-NaF PET represents a unique challenge because there are no clear anatomic references near the heart and because bone motion (where there is significant ^{18}F-NaF uptake) does not correlate with coronary motion. To our knowledge, this is the first report of motion-corrected coronary PET by the use of such nonlinear registration methods.

Our technical development study also has several important implications for the future of coronary ^{18}F-NaF PET imaging, which in its infancy has been hampered by cardiac motion, radiation exposure, and cost. The initial approach to motion was to discard all the PET counts when the heart was moving, resulting in high noise in the end-diastolic PET data. This might ultimately limit the accuracy and clinical utility of ^{18}F-NaF PET in distinguishing true uptake in culprit or high-risk sites from noise-related false-positives. The improved separation of positive from negative lesions and reduction of noise enabled by this motion correction method will likely enhance the capability of ^{18}F-NaF PET and lead to better detection of vulnerable plaques. Our technique retains the count statistics from the full PET acquisition and at the same time increases the TBR as compared with the original 1-bin method. This ultimately may facilitate reduced bed times (improving scan efficiency and reducing costs) or reduced tracer dose and radiation exposure.

In this study, CCTA scans were obtained in the original clinical protocol for the purposes of PET uptake localization and plaque characterization. We opted to use these scans as the anatomic framework for PET motion correction since the data were readily available. To our knowledge, all coronary PET studies (with ^{18}F-NaF or ^{18}F-FDG) to date have used contrast CCTA for localization of PET uptake (*2,19,20*). Registration methods that do not use CCTA could be explored in the future, such as with PET/MR systems. Alternatively, ^{18}F-NaF PET testing could be applied in patients who have already undergone anatomic testing with CCTA and present abnormal results with potentially vulnerable plaques. Under such circumstances, the prior CCTA could be reused (after coregistration to the PET scan or CT attenuation scan obtained with ^{18}F-NaF PET) to localize the ^{18}F-NaF PET uptake and guide motion correction without additional radiation or contrast exposure. Furthermore, we have used the method of Vemuri et al. (*13*) for nonlinear registration of the multiple bins of PET data in the selected coronary regions. This method is computationally efficient, which is important since multiple volume registrations are required for each patient. Other registration algorithms, such as the latest optical flow methods, may have additional benefits that warrant further exploration. Given our demonstration of the feasibility of a nonlinear motion correction method for improved coronary PET imaging, these other approaches and refinements warrant further prospective investigation and validation in future studies.

The incorporation of the CCTA anatomic framework as proposed here can also potentially lead to automation and reproducibility of quantitative analysis of PET uptake, allowing less experienced

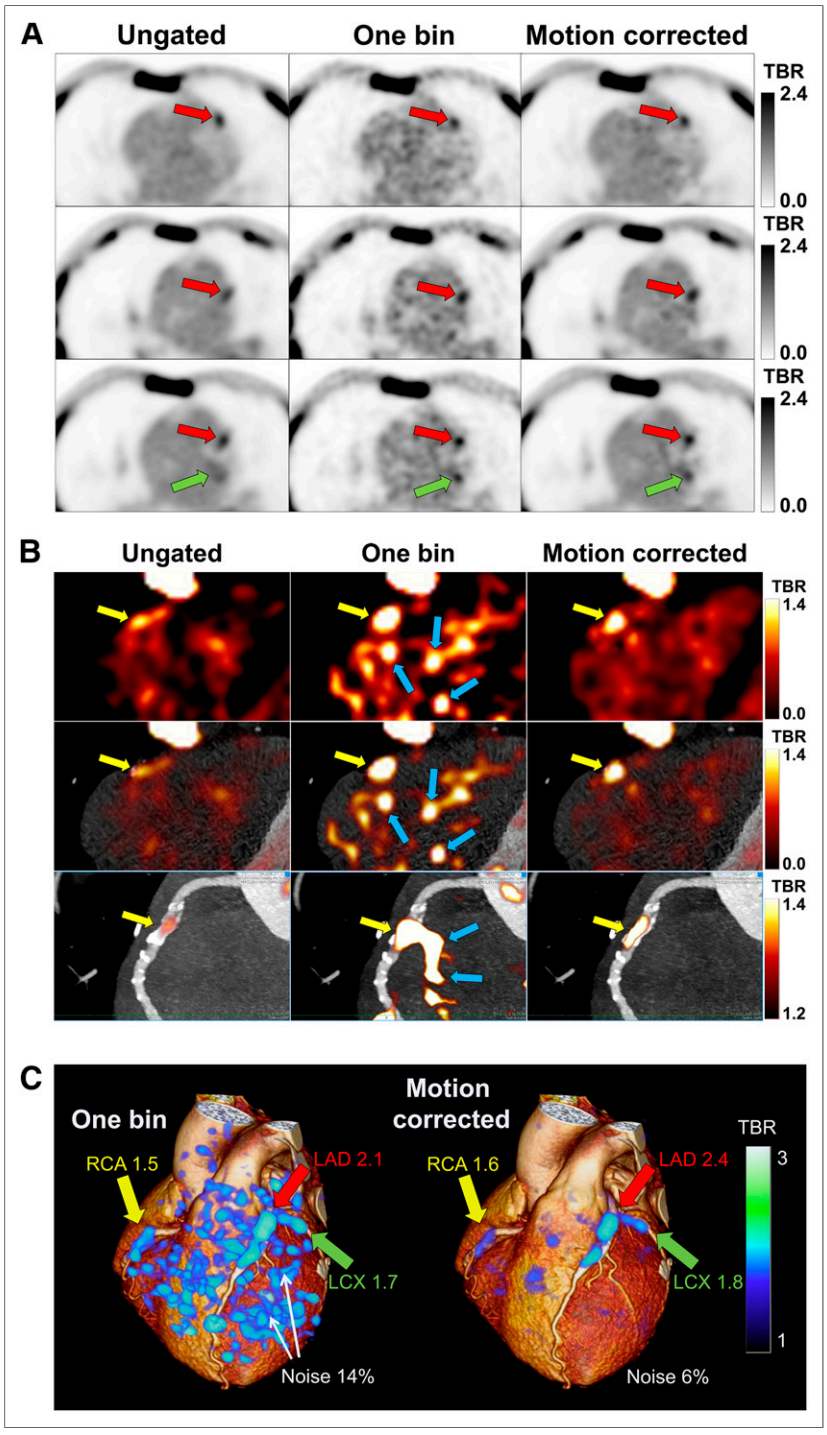

FIGURE 3. Noise decrease and TBR improvement in ^{18}F-NaF PET images of 65-y-old man. (A) On linear grayscale transaxial slices, ^{18}F-NaF plaque uptake is seen in left anterior descending (LAD) (red arrows) and left circumflex (LCX) (green arrows) coronary arteries. The images show blurred lesion signal in ungated images, significant noise in 1-bin images, and high lesion signal with reduced noise in motion-corrected images. (B) On PET (top), PET/CCTA (middle), and multiplanar-reformatted PET/CCTA (bottom) images with exponential color table and same window and level settings, vulnerable plaque is seen in right coronary artery (RCA) (yellow arrows). Low lesion signal is seen in ungated images, significant noise in 1-bin images (blue arrows), and high signal with less noise in motion-corrected images. (C) 3-dimensional rendering of 1-bin image (25% of PET counts) as in study of Joshi et al. (*2*) (left) and motion-corrected image (right) superimposed on rendered CCTA volume. Increased uptake is seen in RCA, LAD, and LCX coronary arteries in high-noise 1-bin image and remains clear in motion-corrected image.

centers to immediately implement this technique and fostering meaningful intercenter comparisons of the data. It is of key importance that this promising PET technique be allowed to reach its full potential by optimizing the image analysis techniques. The CCTA-guided motion correction technique proposed in this work will also be applicable to future PET tracers exploring pathologic processes in the coronary vasculature.

For patients with coronary heart disease, ^{18}F-NaF PET has several applications. First, it may help assess future risk and provide added value to the simple anatomic assessment from CCTA. This may help inform the intensity of medical therapy as well as plan potential coronary revascularization, especially for intermediate lesions or multivessel disease. It may also help determine risk in the context of noncardiac interventions, such as the planning of noncardiac surgery. Finally, it may provide a surrogate biomarker of plaque vulnerability against which novel therapeutic interventions can be assessed.

This study had several limitations. Although it clearly showed significant gains in image quality by the motion correction method applied to ^{18}F-NaF PET imaging, there is room for improvement. Indeed, we are likely to achieve further significant enhancements in TBR by incorporating respiratory and patient motion correction, as well as correction for partial-volume effects. We did not perform these additional corrections in our study because the dual gating and combined correction for these motions is complex. Potentially, PET and CCTA may be misregistered even if CCTA is acquired in end-expiration. Therefore, the CCTA coronary regions may not correspond exactly to the PET regions considered in the motion correction technique. Automatic correction for this alignment may result in further improvements, since our method relies on centerline extraction from the CCTA data, which defines 3-dimensional regions of interest in PET data. Nevertheless, the regions that we used encompassed an approximate coronary artery path neighborhood of 2 cm in diameter, which should allow for some CCTA–PET misregistration. We did not use standardized uptake values (SUVs) in this study, focusing instead on TBR. In our experience, SUV data result in greater variability than TBRs, although this may need to be reevaluated when partial-volume corrections are performed. We acknowledge that the study cohort was small, reflecting the novelty of coronary imaging by ^{18}F-NaF PET. Nevertheless, since there were multiple lesions in each patient, we were able to demonstrate the significant improvements afforded by our technique. We focused on improvement of image quality and discrimination of ^{18}F-NaF PET–positive lesions from ^{18}F-NaF PET–negative lesions, rather than on the clinical utility of coronary ^{18}F-NaF PET. An ongoing prospective

study (NCT02278211) aims to demonstrate the value of coronary ^{18}F-NaF PET in predicting future myocardial infarction (*21*). When this trial is completed, we plan to apply the techniques to demonstrate improved prediction of myocardial infarction.

CONCLUSION

Motion correction of gated ^{18}F-NaF PET/CT reduces noise and increases TBR as compared with 1-bin imaging and further improves TBR as compared with ungated images without a noise increase. This improvement may allow more reliable identification of vulnerable plaque lesions in the coronary arteries by ^{18}F-NaF PET.

DISCLOSURE

The costs of publication of this article were defrayed in part by the payment of page charges. Therefore, and solely to indicate this fact, this article is hereby marked "advertisement" in accordance with 18 USC section 1734. The study was funded by the Chief Scientist Office, Scotland (ETM/160). David Newby (CH/09/002) and Marc Dweck (FS/14/78) are supported by the British Heart Foundation. David Newby is the recipient of a Wellcome Trust Senior Investigator Award (WT103782AIA). The study was also supported in part by a grant (Cardiac Imaging Research Initiative) from the Adelson Medical Research Foundation at Cedars-Sinai. Piotr Slomka and Daniel Berman receive research grant support from Siemens Medical Systems. No other potential conflict of interest relevant to this article was reported.

REFERENCES

1. Mozaffarian D, Benjamin EJ, Go AS, et al. Heart disease and stroke statistics: 2015 update—a report from the American Heart Association. *Circulation.* 2015; 131:e29–e322.
2. Joshi NV, Vesey AT, Williams MC, et al. ^{18}F-fluoride positron emission tomography for identification of ruptured and high-risk coronary atherosclerotic plaques: a prospective clinical trial. *Lancet.* 2014;383:705–713.
3. Dweck MR, Chow MW, Joshi NV, et al. Coronary arterial ^{18}F-sodium fluoride uptake: a novel marker of plaque biology. *J Am Coll Cardiol.* 2012;59:1539–1548.
4. Irkle A, Vesey A, Lewis D, et al. Identifying active vascular microcalcification by ^{18}F-sodium fluoride positron emission tomography. *Nat Commun.* 2015;6:7495.
5. Gigengack F, Ruthotto L, Burger M, Wolters CH, Jiang X, Schafers KP. Motion correction in dual gated cardiac PET using mass-preserving image registration. *IEEE Trans Med Imaging.* 2012;31:698–712.
6. Lamare F, Le Maitre A, Dawood M, et al. Evaluation of respiratory and cardiac motion correction schemes in dual gated PET/CT cardiac imaging. *Med Phys.* 2014;41:072504.
7. Slomka PJ, Nishina H, Berman DS, et al. "Motion-frozen" display and quantification of myocardial perfusion. *J Nucl Med.* 2004;45:1128–1134.
8. Le Meunier L, Slomka PJ, Dey D, et al. Motion frozen ^{18}F-FDG cardiac PET. *J Nucl Cardiol.* 2011;18:259–266.
9. Lesage D, Angelini ED, Bloch I, Funka-Lea G. Bayesian maximal paths for coronary artery segmentation from 3D CT angiograms. *Med Image Comput Comput Assist Interv.* 2009;12:222–229.
10. Schuhbaeck A, Dey D, Otaki Y, et al. Interscan reproducibility of quantitative coronary plaque volume and composition from CT coronary angiography using an automated method. *Eur Radiol.* 2014;24:2300–2308.
11. Dey D, Achenbach S, Schuhbaeck A, et al. Comparison of quantitative atherosclerotic plaque burden from coronary CT angiography in patients with first acute coronary syndrome and stable coronary artery disease. *J Cardiovasc Comput Tomogr.* 2014;8:368–374.
12. Diaz-Zamudio M, Dey D, Schuhbaeck A, et al. Automated quantitative plaque burden from coronary CT angiography noninvasively predicts hemodynamic significance by using fractional flow reserve in intermediate coronary lesions. *Radiology.* 2015;276:408–415.
13. Vemuri BC, Ye J, Chen Y, Leonard CM. Image registration via level-set motion: applications to atlas-based segmentation. *Med Image Anal.* 2003;7: 1–20.
14. Shechter G, Resar JR, McVeigh ER. Displacement and velocity of the coronary arteries: cardiac and respiratory motion. *IEEE Trans Med Imaging.* 2006;25:369–375.
15. Martinez-Möller A, Souvatzoglou M, Navab N, Schwaiger M, Nekolla SG. Artifacts from misaligned CT in cardiac perfusion PET/CT studies: frequency, effects, and potential solutions. *J Nucl Med.* 2007;48:188–193.
16. Koivumäki T, Nekolla SG, Furst S, et al. An integrated bioimpedance–ECG gating technique for respiratory and cardiac motion compensation in cardiac PET. *Phys Med Biol.* 2014;59:6373–6385.
17. Hong I, Jones J, Casey M. Elastic motion correction for cardiac PET studies. Presented at: Nuclear Science Symposium and Medical Imaging Conference; Seoul, Korea; 2013.
18. Slomka PJ, Rubeaux M, Le Meunier L, et al. Dual-gated motion-frozen cardiac PET with flurpiridaz F18. *J Nucl Med.* September 24, 2015 [Epub ahead of print].
19. Cheng VY, Slomka PJ, Le Meunier L, et al. Coronary arterial ^{18}F-FDG uptake by fusion of PET and coronary CT angiography at sites of percutaneous stenting for acute myocardial infarction and stable coronary artery disease. *J Nucl Med.* 2012;53:575–583.
20. Rogers IS, Nasir K, Figueroa AL, et al. Feasibility of FDG imaging of the coronary arteries: comparison between acute coronary syndrome and stable angina. *JACC Cardiovasc Imaging.* 2010;3:388–397.
21. Newby DE, Dweck M. Prediction of recurrent events with ^{18}F-fluoride (PREFFIR). ClinicalTrial.gov website. https://clinicaltrials.gov/ct2/show/NCT02278211. Received October 14, 2014. Updated May 26, 2015. Accessed October 21, 2015.